JOURNAL OF GEOPHYSICAL RESEARCH, VOL. 105, NO. B7, PAGES 16,193–16,205, JULY 10, 2000

D" as a transition in the heterogeneity spectrum of the lowermost mantle

Vernon F. Cormier

Department of Geology and Geophysics, University of Connecticut, Storrs

Abstract. Broadband *SH* and *P* wave fields are pseudospectrally modeled in three forms of the heterogeneity spectrum of the mantle, each having a transition in the power spectrum of heterogeneity in the lowermost mantle. With D" defined as a zone of increased heterogeneity, low-pass and high-pass filters of models of the heterogeneity spectrum demonstrate that the thickness of D" inferred from an incident seismic wave field can depend on the dominant wavelength of that wave field. A model of D" heterogeneity that agrees with the coda power between *S* and *ScS* and between *P* and *PcP* is a simple linear extrapolation of the spectrum of heterogeneity power versus depth determined from global tomography to wavenumbers corresponding to short-period body waves. The negligible decay in the power spectrum of heterogeneity across a band of wavenumbers from 0.0001 to 1 km^{-1} is consistent with a pervasive entrainment of small scale chemical heterogeneities by convective motions. The lack of strong scattering attenuation in observed *ScS* and *PcP* waveforms is used to establish upper bounds in this wavenumber band of 3% and 1.5% on the root-mean-square variations of *S* and *P* velocity, respectively. Some realizations of the preferred model of the heterogeneity spectrum generate an *SdS* waveform from scattering by an elongated, high velocity anomaly, roughly parallel to the core-mantle boundary. The high topography of similarly shaped anomalies needed to account for the amplitude of narrow angle scattering observed from D" argues against such anomalies having the high-density perturbation expected for a chemically distinct or phase-transformed layer.

1. Introduction

Lateral heterogeneity and anisotropy of the lowermost 200 to 1000 km of the mantle is well documented over a broad range of scale lengths, ranging from thousands of kilometers from travel time tomography [*Su et al.*, 1994] to 10 km or less from waveform complexity [*Bataille et al.*, 1990]. Knowledge of the fabric of the heterogeneity of the lower mantle is important to models of convection, including the possibility of plumes originating at the core-mantle boundary, models of slab penetration into the deep mantle, and models of chemical heterogeneity.

It is quite possible that the Earth's lowermost mantle is as structurally complex as its upper mantle and crust. Much of this complexity, however, may be hidden from view with the imaging techniques commonly applied to seismic waves having zones of sensitivity equal to and larger than the scale lengths of the heterogeneous structures in this region. It is also clear that the domain of scale lengths (sometimes 1 km or less) needed to understand the detailed processes of possible partial melting or chemical reaction at the base of the mantle will remain inaccessible to travel time tomography. To resolve or at least constrain the statistics of these small-scale lengths, an important tool of the future may involve waveform modeling in two- and three-dimensional models having a continuous spatial spectrum of heterogeneity from scales of kilometers to thousands of kilometers. With sufficiently dense profiles of data, such numerical modeling may eventually become a routine component of waveform tomography.

Paper number 2000JB900141.
0148-0227/00/2000JB900141$09.00

2. Modeling Technique

The scale lengths of heterogeneity considered in this paper span the domain in which descriptions of statistical properties of the medium merge with deterministic descriptions. To investigate accurately the effect of heterogeneities in a domain of scale lengths that encompass such a broad passband, it is best to use a fully numerical solution of the elastic equations of motion.

2.1. Pseudospectral Method and Its Implementation

To accomplish this, a two-dimensional pseudospectral approach is taken. Like the standard finite difference approach, the pseudospectral approach numerically in-

tegrates the equations of motion in time, but computes spatial derivatives by Fourier transforms. The names pseudospectral and collocation are generally applied to any method in which spatial derivatives of linear differential equations are handled in a transform domain [*Fornberg,* 1996]. Although computationally more expensive than even an eighth-order finite difference method, pseudospectral methods offer superior accuracy and minimal sampling to achieve minimum grid dispersion [*Kosloff and Kessler,* 1990]. Minimizing grid dispersion is an especially important requirement in a teleseismic application, which requires accurate propagation of the seismic wavefield over thousands of wavelengths.

Two-dimensional pseudospectral codes were parallelized and implemented on a multiprocessor system. The storage of model parameters was distributed by stripes assigned to different processors (Figure 1). A transpose routine was used to convert storage between horizontal and vertical stripes for spatial derivatives taken by the Fourier method in the horizontal direction and the vertical direction, respectively. Since all of the interprocessor communication takes place in the transpose operation, considerable savings can be achieved by optimizing the transpose routine. The transpose routine employed the Message Passing Interface (MPI) parallel library [*Snir et al.,* 1998] to define structures of new data types to perform the transpose with a single call to MPI_ALLTOALL.

A velocity-stress formulation is applied on a staggered grid [*Virieux,* 1986], equivalent to the spatial shifting by half grid samples with power of two fast Fourier transforms (FFTs) described by *Witte* [1985]. In all *SH* profiles, an *SH* line source is assumed at a depth of 500 km, and a line to point source correction is applied to all figures showing displacement waveforms. The *P* profile discussed in section 3.5 assumes a point body force acting in a vertical direction. *SH* profiles have a constant spatial sampling of $\Delta x = \Delta z = 10$ km, corresponding to a 5 km half sampling rate of parameters on a staggered grid. The *P* profile has a radial sampling $\Delta r = 6$ km and an angular sampling $\Delta\theta = 0.0016$. These intervals of spatial sampling are close to the densest sampling intervals that *Furumura et al.* [1998] used in the vicinity of velocity and density discontinuities. Absorbing boundary conditions are avoided on the sides of the model by summing the results of periodic and antiperiodic wave fields [*Furumura and Takenaka,* 1995]. The codes have an option for arbitrary frequency dependence of anelasticity using sums of relaxation functions [*Robertsson et al.,* 1994; *Blanch et al.,* 1995]. Intrinsic anelasticity has been included in the *P* profile shown in section 3.5 but not in the *SH* profiles. The complete record section and wavefronts shown in Figure 2 are similar to results shown by *Igel and Weber* [1996] and *Furumura et al.* [1998].

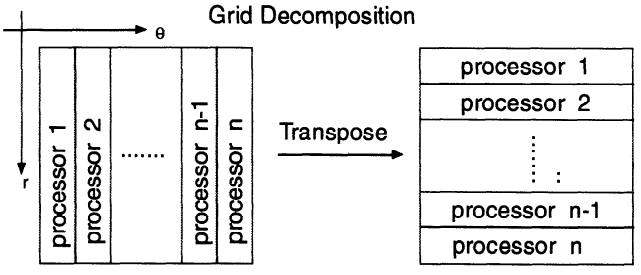

Figure 1. Grid decomposition scheme for implementing the pseudospectral method on a multiprocessor system. Spatial derivatives are performed in parallel for the vertical stripes, the grid decomposition is transposed from vertical stripes to horizontal stripes, and spatial derivatives are calculated in parallel for horizontal stripes. A transpose operation is applied again to restore the grid decomposition to vertical stripes for the next time step.

2.2. Model Construction

All models start with the preliminary reference Earth model (PREM) [*Dziewonski and Anderson,* 1981] as a reference model, in which the crust has been removed. Perturbations to PREM are constructed using the procedure described by *Frankel and Clayton* [1986]. In this procedure, pseudo-random numbers are assigned to grid points of the model, and the model is Fourier transformed to wavenumber space, filtered by an assumed wavenumber spectrum, and inverse Fourier transformed back to space.

Evidence exists for mantle heterogeneity at scale lengths as long as 10,000 km [e.g., *Su et al.,* 1994] and as short as 10 km [e.g., *Hedlin et al.,* 1997]. The heterogeneity power observed at these two extremes in scale lengths is similar, of the order of 0.5 to 2%. Although it is not known whether the heterogeneity spectrum is continuous between these two extremes of scale lengths, it is reasonable, at least initially, to assume a relatively white spectrum across a broad band of wavenumbers, having a decay with increasing wavenumber no faster than k^{-1} to k^{-2}. These constraints are met by assuming an exponential autocorrelation of *S* velocity perturbation ($\Delta V_S/V_S$) with a critical scale length in the horizontal and vertical directions between 20 km and 400 km. At spatial scales below this critical scale length an exponential autocorrelation gives a nearly white wavenumber spectrum. At scales shorter than this critical scale length the 2-D power spectrum decays like $k^{-1.5}$, corresponding to a k^{-2} decay in a 3-D Earth. Any other parameterization of autocorrelation is satisfactory as long as it gives sufficient power over a broad band of scale lengths.

In the *P-SV* modeling in section 3.5, $dlnV_S/dlnV_P$ is assumed equal to 2. The density perturbations associated with the deep heterogeneities of the Earth are assumed to be much smaller than their perturbations in seismic velocities and are set to zero.

An Earth flattening approximation (EFA) is applied to the 2-D models in which the *SH* wave field is calcu-

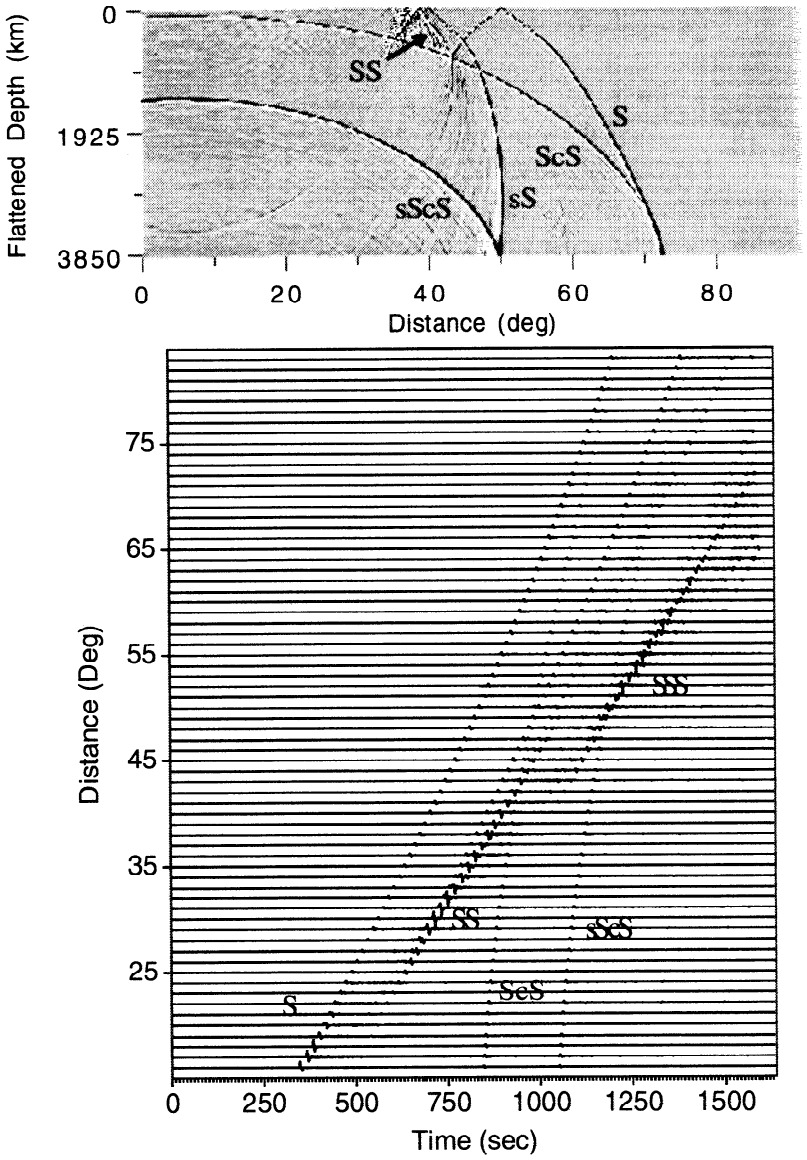

Figure 2. (top) Snapshot of *SH* particle velocity at t = 819.2 s, showing *S*, *sS*, *SS*, *ScS*, and *sScS* wavefronts for an *SH* line source at 500 km depth and 610 km from the left side of a staggered grid with $nx = nz$ =1024 and $\Delta x = \Delta z = 10$ km. The complete calculation used 32,768 time steps with $\Delta t = 0.05$ s. (bottom) Record section of *SH* velocity waveforms for receivers at the surface.

lated. The EFA is known to be exact for *SH* waves in a vertically heterogeneous medium [*Chapman,* 1973] but results in horizontal scales of heterogeneity decreasing proportionally with radius as radius decreases. Thus, for example, a 20 km scale length of heterogeneity in a flattened model is equivalent in a spherical model to a 20 km scale length at the surface, but a 11 km scale length at the core-mantle boundary. Correction for this effect is included in references to specific scale lengths in section 3. The initial work for the *SH* wave field shown in this paper used an EFA for greater simplicity in the generation of random model perturbations by the Fourier methods of *Frankel and Clayton* [1986]. For accuracy, the profile of *P* waves in section 3.5 used cylindrical coordinates.

3. Results

The *SH* wavefield has been synthesized in several different Earth models having either a change in the shape, power, or anisotropy of the heterogeneity spectrum in the D" region of the mantle. Thus far, three types of change of heterogeneity statistics in D" have been tested for effects on broadband *S* + *ScS* (Figure 3 and Plate 1).

3.1. D" as a Transition From Isotropy to Anisotropy of Scale Lengths

Model 1 of D" heterogeneity (Figure 3 (top) and Plate 1 (top)) has an abrupt (40 km) transition from an isotropy of scale lengths of heterogeneity to horizontally elongated heterogeneity. This type of transition would

be consistent with a transition to either (1) a dominantly horizontal convective flow near the core mantle boundary that orients macroscopic heterogeneities, (2) flat lying, horizontally stratified, remnants of subducted slab, or (3) horizontally oriented lenses of partial melt.

Plate 1 (top) shows a 2500 x 2500 km patch of the model, including its appearance through filters that low pass and high pass its wavenumber spectrum. The actual model used in calculations is ~5 times larger (10 km x 1024 nodes) on each side, with the velocity perturbation periodically repeating in the horizontal direction, for propagation experiments to ~90° range.

Model 1 was designed to satisfy constraints given by scattered precursors to *PKIKP* [*Cormier,* 1999]. That study found that short period precursors to *PKIKP* are relatively insensitive to elongated (100 km and greater) anomalies parallel to the core-mantle boundary. To account for the shape of the coda to *PKIKP* precursors, such horizontally elongated heterogeneity must be superposed by a component of small-scale (10 km) isotropic heterogeneity. Broadband and long period precursors to *PKIKP* constrain the intensity of horizontally stretched heterogeneity to ~2% perturbation of P velocity or ~2-6% in S velocity [*Cormier,* 1999]. Synthetic seismograms in a model having anisotropy of scale lengths of this type in D" have a coherent feature between S and ScS (Figure 4) that could be identified as a wide-angle reflection by a discontinuity. The abruptness of change in heterogeneity statistics needed to produce this reflection is consistent with either a change in composition or a change in solid phase. The waveform and timing of this reflection, however, do not provide a good match to observations of the feature often observed between S and ScS [*Lay and Helmberger,* 1983]. The magnitude of velocity perturbation (2%) in the D" lamellae of this model is also too small to explain the observed transverse isotropy of D" by shape-preferred orientations [*Kendall and Silver,* 1998].

3.2. D" as a Transition in the Power of the Heterospectrum at Long Scale Lengths

Model 2 (Figure 3 (middle) and Plate 1 (middle)) was motivated by *Shearer et al.'s* [1998] work on *PKIKP* precursors. Their study found a 1% heterogeneity existing everywhere in the lower mantle in the 0.3-0.5 km^{-1} wavenumber band, without D" showing any strong enrichment in D" heterogeneity. Other data considered in the construction of this model come from convective

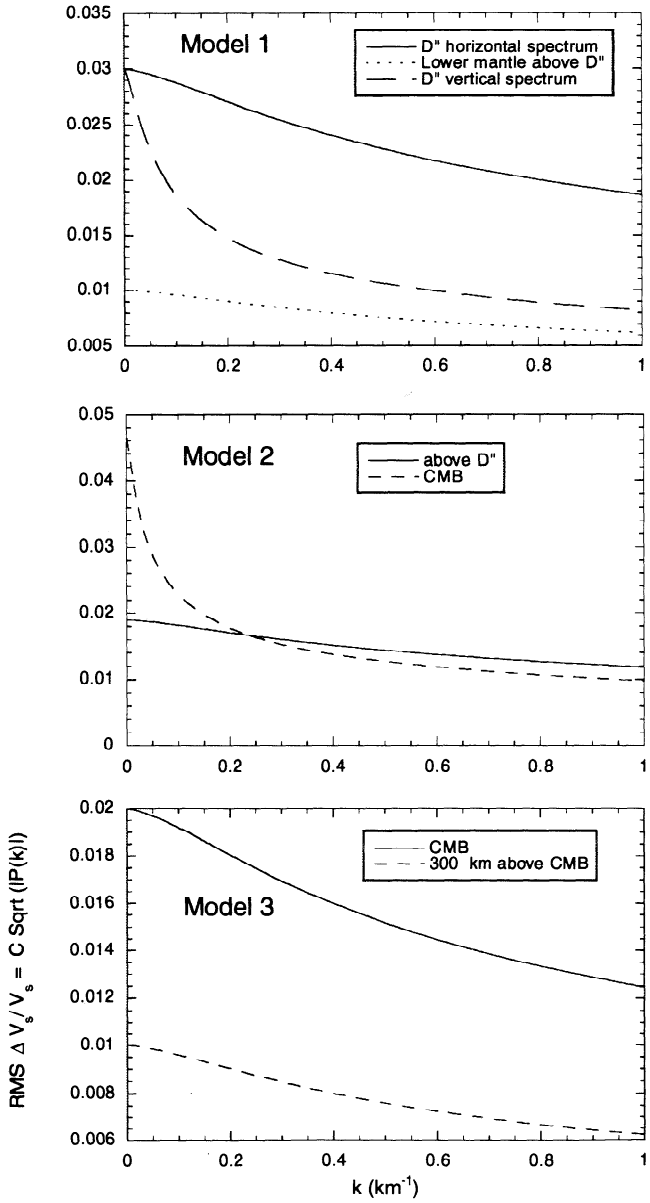

Figure 3. Wavenumber spectra of models of lower mantle heterogeneity. The constant C, which multiples the square root of the amplitude of the power spectrum in the caption of the ordinate axis, is chosen to give specified RMS values of velocity fluctuation $\Delta V_S/V_S$ after the complex wavenumber spectrum is transformed back into space. (top) The wavenumber spectrum of model 1 has an exponential, spatially isotropic, autocorrelation with a 20 km scale length and a 1% RMS fluctuation in $\Delta V_S/V_S$ in the lower 1000 km of the mantle. In the lowermost 300 km of the mantle a 2% RMS $\Delta V_S/V_S$ fluctuation is added having an exponential, spatially anisotropic autocorrelation. The spatial anisotropy, specified by parameters that control the corner frequency of the wavenumber spectrum, has a 20 km scale length in the vertical direction and 200 km scale length in the horizontal direction. (middle) Wavenumber spectra of model 2 have an exponential, spatially isotropic, autocorrelation with a 20 km scale length and a RMS $\Delta V_S/V_S = 1.2\%$ in the mantle above D". In D" a gradient transition occurs, which increases the RMS perturbation to $\Delta V_S/V_S$ to 5% and reddens the corner scale length to 400 km at the core-mantle boundary (CMB). (bottom) The wavenumber spectrum of model 3 has an exponential, spatially isotropic, autocorrelation with a 10 km scale length in the lower mantle. Starting 300 km above the core-mantle boundary, the power of velocity perturbation increases by a linear gradient from $\Delta V_S/V_S$ equal to 1% to $\Delta V_S/V_S$ equal 3% at the core-mantle boundary.

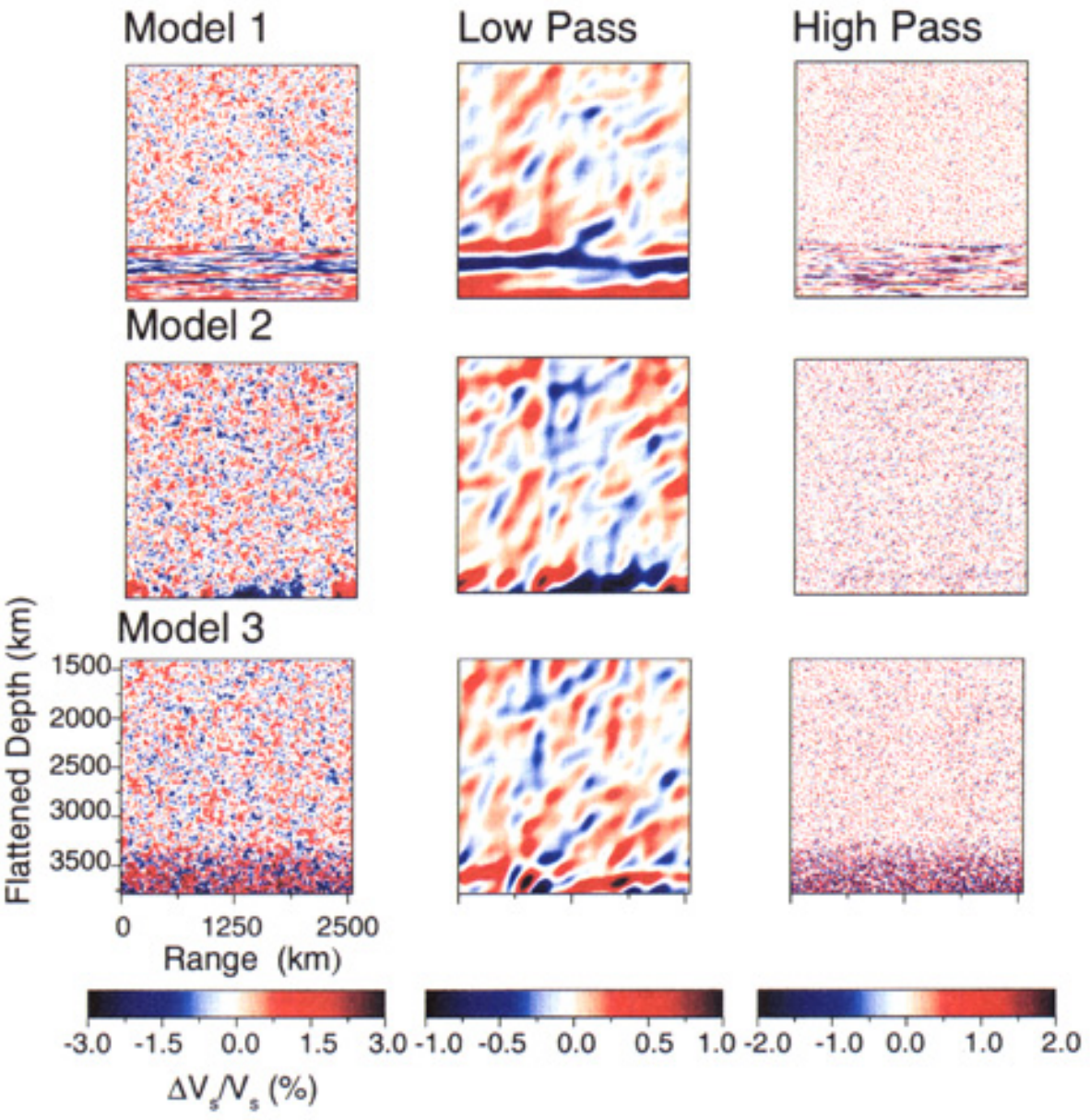

Plate 1. (top) Images of model 1 lower mantle structure. The low-passed structure removes all heterogeneities having scale lengths shorter than 200 km. The high- passed structure removes all heterogeneities having scale lengths longer than 20 km. (middle row) Images of model 2 lower mantle structure. Note how D" disappears as a distinct feature in the high-passed image. (bottom row) Images of model 3 lower mantle structure.

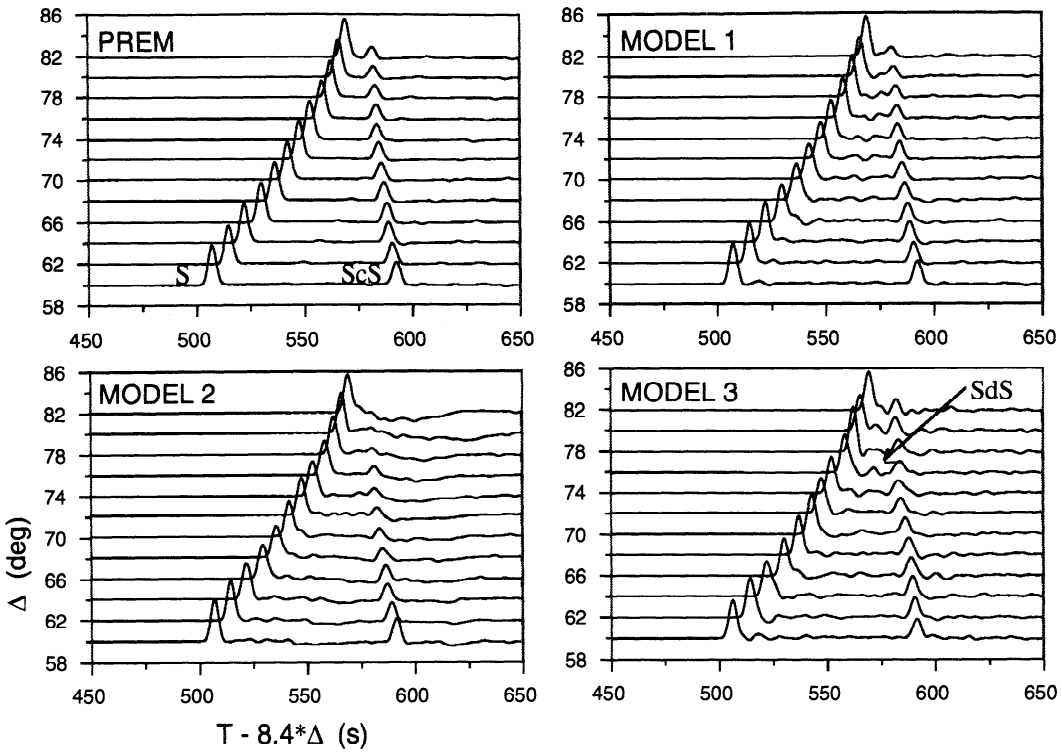

Figure 4. *SH* displacement synthetic seismograms for PREM [*Dziewonski and Anderson,* 1981] and models 1-3 of lower mantle heterogeneity. Note how *ScS* suffers severe attenuation due to the strong heterogeneity power of model 2 near the core- mantle boundary, and note *SdS* arrivals between *S* and *ScS* in model 3.

[*Tackley,* 1998] and tomographic modeling [*Dziewonski,* 1995], which suggest a reddening of the heterospectrum in D" at small wavenumbers in the lower mantle. More specifically, global tomography gives an indication of a reddening of the spatial spectrum of heterogeneity in both the lower and upper mantle, with a white spectrum of heterogeneity in the midmantle up to harmonic order 10-12. These harmonic orders correspond to scale lengths on the order of 2000 km [*Dziewonski,* 1995].

Compared to the midmantle, model 2 increases the power of heterogeneity at long scale lengths, while keeping the power of heterogeneity at short scale lengths similar to the midmantle. Patches of high-velocity and low-velocity regions at the core-mantle boundary are seen with the low-pass filter of this model. The D" region, however, disappears as a distinct layer in the high-pass filter (Plate 1 (middle)). This type of model could thus account for the lack of evidence for a globally thin D" layer in *PKIKP* precursor data in the short-period band. It could also simultaneously account for observations of D" discontinuities and ultra low-velocity zones in long-period data through the effects of lamellae having long scale lengths parallel the core-mantle boundary.

Synthetic seismograms (Figure 4), however, show that this type of model fails to produce an *SdS* arrival and attenuates *Sc*S too much. Apparently, the power in long horizontal scale lengths in the D" region of this model has led to strong stratigraphic attenuation [e.g., *Richards and Menke,* 1983] of core-grazing *ScS*. Although occasional reports of increased attenuation in D" cannot be yet discounted [*Anderson and Given,* 1982], the level of observed attenuation is too small to be consistent with the highly attenuated *ScS* waves shown in Figure 4. The observed amplitude of long-period *ScS* in the 80°-90° range is consistent with an upper bound of 2-3% in S velocity heterogeneity in D" the 0.01 to 1.0 km^{-1} wavenumber band. Thus it is impossible to construct a successful model having a reddening of the heterogeneity spectrum in the lowermost mantle by keeping the heterogeneity power at small-scale lengths equal to that in the midmantle.

Reddening, relative to the midmantle, can only be accomplished by reducing power at short scale lengths, which would then be inconsistent with observations of scattered precursors to short-period *PKIKP*. The next numerical experiment assumes no substantial reddening occurs between the between the wavenumber band resolved by global tomography and the 0.01 to 1 km^{-1} band.

3.3. D" as a Transition in the Power of Heterogeneity at All Scale Lengths

Model 3 (Figure 3 (bottom) and Plate 1 (bottom)) was constructed by simply assuming that the tomograhically resolved S velocity heterospectrum (Figure

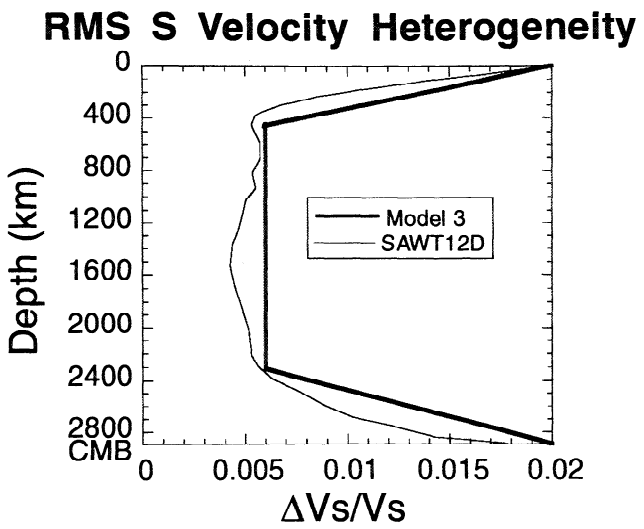

Figure 5. Model 3 of lower mantle heterogeneity is based on models of mantle heterogeneity determined from global tompography, such as SAWT12D of *Li and Romanowicz* [1996], having higher heterogeneity in both the upper and lower mantle, with gradient transitions in the intensity of heterogeneity.

5) can be linearly extrapolated to short scale lengths. This extrapolation assumes a white or slowly decaying spectrum between scale lengths 0.002 and 1 km^{-1}. Three line segments were fit through the plots of the root-mean-square S velocity fluctuation versus depth shown in the tomographic study of *Li and Romanowicz* [1996]. This resulted in a model having a decreasing intensity of velocity fluctuation from the surface to 670 km depth, a region of constant intensity of velocity fluctuation from 650 km depth to 350 km above the core-mantle boundary, and increasing intensity of velocity fluctuation in the D" region. Specifically, a 0.6% RMS fluctuation of $\Delta V_S/V_S$ in the midmantle is assumed to linearly increase in intensity with increasing depth, starting at 350 km above the core-mantle boundary, to a 2% RMS fluctuation of $\Delta V_S/V_S$ at the core-mantle boundary (CMB).

Note in Plate 1 that D" low-velocity and high-velocity patches at the CMB are observed in the low-pass-filtered model. In the high-pass-filtered version, a slight enrichment of small-scale heterogeneity can be discerned. Peak velocity fluctuations are typically more than a factor of 2 higher (5% or more) than the velocity fluctuation measured by the RMS fluctuation (2%).

In the synthetics (Figure 4), a *SdS* arrival is created having a surprising coherence for 4° or more and bearing strong resemblance to data (Figure 6). Also note in Figure 4 the polarity reversal of *SdS* in model 3 at 74° and some broadening of *ScS*. In additional experiments, in which the intensity of the heterogeneity in D" in this type of model was doubled, *ScS* became highly broadened and attenuated. These results are again consistent with the upper bound of ~2 to 3% in D" for *S* velocity RMS perturbations in the 0.002 to 1 km^{-1} wavenumber band.

The success of this model in matching observations of an apparent wide-angle reflection between *S* and *ScS* motivated further experiments to understand what features of heterogeneous structure are responsible for waveform features that mimic the effects of layered structure. Two more realizations of model 3 were generated, and *SH* seismograms were synthesized in those models (Figure 7). Although these synthetic waveforms have a similar level complexity between *S* and *ScS*, only one of these realizations produces a coherent *SdS* phase similar in character to observations.

Cross sections of the model realizations were low pass filtered (Plate 2) to examine what feature may responsible for generating a coherent *SdS* arrival. Plate 2 suggests that the responsible feature is an elongated high-velocity anomaly, roughly parallel to the core-mantle boundary, centered above the ray theoretical reflection point of *ScS*, spanning the Fresnel zone of long-period body waves that may be scattered by the anomaly. A feature in vertical profiles through this anomaly (Figure 8), shared with 1-D models that predict an *SdS* phase, is an abrupt velocity increase followed by a negative gradient with increasing depth. The depth of the feature responsible for *SdS* is ~100 km closer to the core-mantle boundary than the feature in 1-D models such as SYLO. At least some of the difference in the depth of the high velocity responsible for *SdS* compared between model 3 and SYLO may be due to the effects of lateral variations in the shape of the high-velocity anomaly. Lateral undulations in the high velocity anomaly may scatter energy into a later time window than would a later-

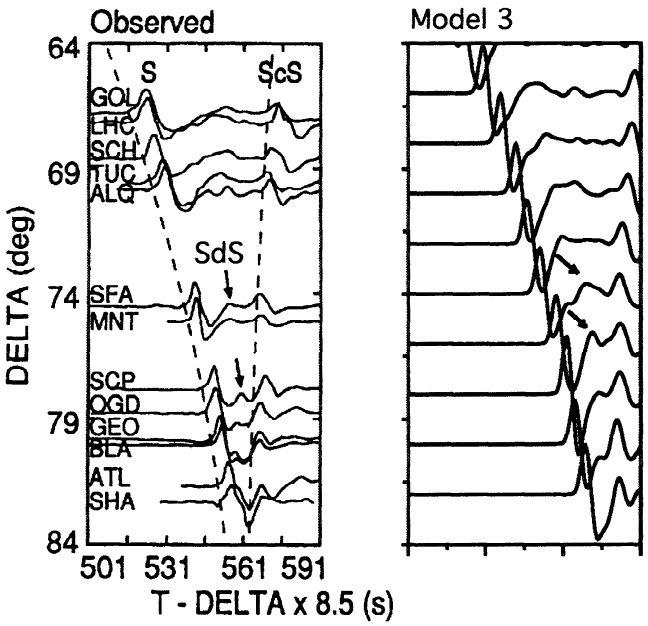

Figure 6. (left) Long-period World-Wide Standardized Seismograph Network (WWSN) observations of *SH* waveforms from *Lay and Helmberger* [1983] compared with (right) synthetic seismograms for model 3 convolved with a long- period WWSSN instrument response.

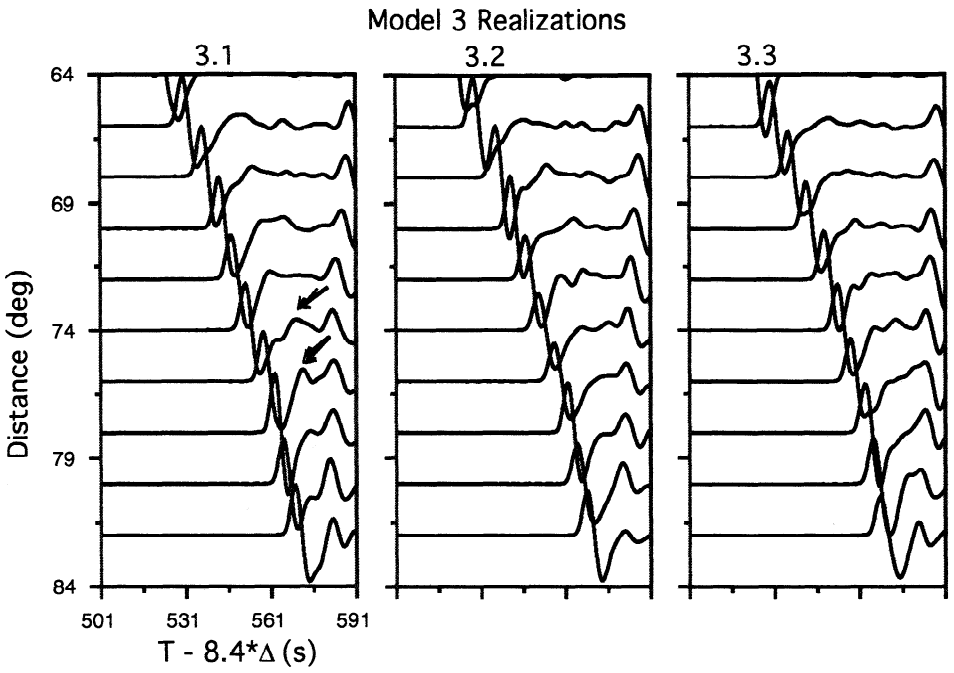

Figure 7. Long-period WWSSN convolved synthetic seismograms for three different realizations of the model 3 heterogeneity spectrum.

ally homogeneous anomaly, making it appear as if the wide-angle reflection originates from a higher, laterally homogeneous anomaly.

3.4. Observations of Narrow Angle Reflections From the D" Region

None of the three types of 2-D heterogeneous models described in this paper produces observable narrow angle reflections from heterogeneities in the lowermost mantle (Figure 9), which arrive as precursors to *ScS* in the 10° to 30° range [*Schimmel and Paulssen,* 1996]. Model 3, however, predicts some pulse broadening of *ScS* and some complexity in its postcursory coda, which may be useful for constraining D" heterogeneity in comparisons with observed *ScS* waveforms. The lack of a strong, coherent, precursor in model 3 synthetics might be due to differences in the predictions of 2-D versus 3-D simulations or, more likely, due to neglect of possible lateral variation in the depth of onset of a change in heterogeneous statistics. In each of the models tested thus far, this onset depth has been kept laterally constant at a value between 200 and 700 km from the CMB. It is difficult to make a *ScS* precursor having amplitude as high as 10% that of *ScS* in the 10° to 30° range without allowing for considerable topography in this onset depth. The curvature of the boundaries of extended high-velocity anomalies should be as least as strong as the curvature of the incident S wave front at the CMB, and possibly strong enough to cause critical reflection of steeply incident *S* waves. In a discontinuity interpretation, *Schimmel and Paulssen* [1996] find a scale length of topography between 1200 and 1600 km and a height variation on the order of 50 km. In a statistical interpretation of D" structure these parameters would apply to the lateral and vertical onset of a rapid change in the heterogeneity spectrum.

3.5. *P* Plus *PcP* Profile in Model 3

A $dlnV_S/dlnV_P$ scaling equal to 2 is assumed in model 3 and the *P-SV* wave field is calculated for a vertical point force. Figure 10 shows the results for the vertical component of motion for *P* plus *PcP* in the distance range 58° to 84°. No coherent reflection from D" anomalies is observed between *P* and *PcP*. Model 3 with this $dlnV_S/dlnV_P$ scaling is thus consistent with the less frequent observation of *PdP* phases [*Wysession et al.,* 1998]. As in the case of *ScS*, pulse broadening of *PcP* due to scattering can be used to place an upper bound of ~1-2% on $\Delta V_P/V_P$ heterogeneity in D" in the 0.01 to 1 km^{-1} wavenumber band. This upper bound is consistent with the results obtained from the analysis of scattered precursors to *PKIKP* [*Hedlin et al.,* 1997; *Shearer et al.,* 1998; *Cormier,* 1999].

4. Discussion

4.1. Nonuniqueness of Models for Excitation of *SdS* and *PdP* Phases

Several very different types of changes in heterogeneity statistics in D" are found to generate coherent *SdS* arrivals between *S* and *ScS*. Among these models is the three-dimensional low-velocity anomaly suggested by *Haddon and Buchbinder* [1987], who showed that diffractions from a three-dimensional, plume-like structure can produce realistically coherent *SdS* phase.

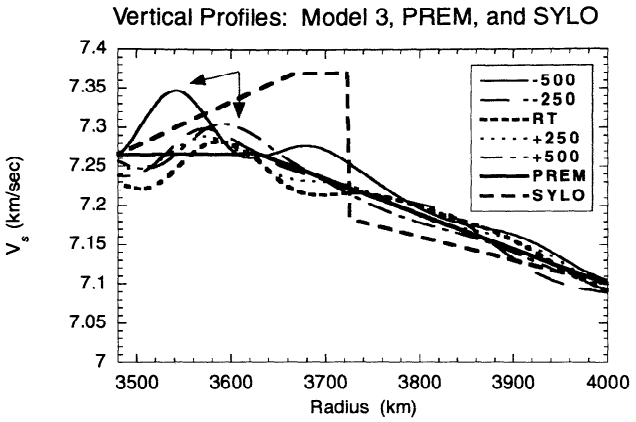

Figure 8. Vertical profiles of S velocity through PREM, SYLO, and a laterally heterogeneous model 3. Vertical profiles for model 3 are shown through the ray theoretical reflection point (RT) of *ScS* on the core-mantle boundary and through points displaced 500 and 250 km to either side of point RT.

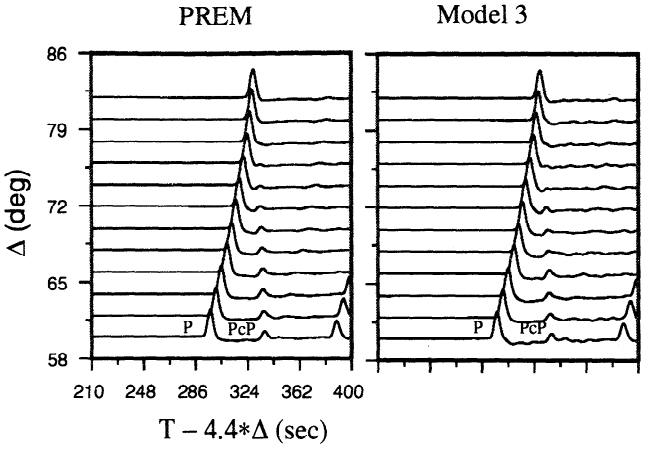

Figure 10. P plus PcP displacement for PREM and model 3. The vertical component of motion is shown for a vertical point source. Note how the distortion and broadening of PcP in model 3, particularly near 68°, mimics the effects expected for low intrinsic Q in D".

In the current study, two-dimensional models whose low-passed wavenumber structure have elongated high-velocity anomalies embedded in a low-velocity region are most successful in producing the observed signature of *SdS*. In this feature, these 2-D models are similar to the original 1-D SYLO model proposed by *Lay and Helmberger* [1983]. The lateral undulations of such a structure in a 2-D model, however, may make it appear as if wide-angle reflections are originating from a 1-D discontinuity located slightly higher above the core-mantle boundary. This apparent depth discrepancy together with *Haddon and Buchbinder's* [1987] 3-D demonstration and the observations of strong topography on an apparent D" reflector or scatterer emphasize that full 3-D imaging and modeling will be necessary to obtain a good understanding of D" structure.

Strong topography of elongated high-velocity anomalies is needed to reconcile both wide-angle and narrow-angle reflection. Such topography argues against a solid phase transition [*Sidorin et al.*, 1999], which would occur over a narrow range of pressure and temperature, or a chemically distinct layer, which would be accompanied by density changes with buoyancy limiting topography on its boundary [*Kellogg*, 1997]. Remaining, viable, alternative origins for elongated anomalies, roughly parallel to the core-mantle boundary, are slab remnants, mixed bands of core-mantle reaction products, or bands of partial melts. Each of these alterna-

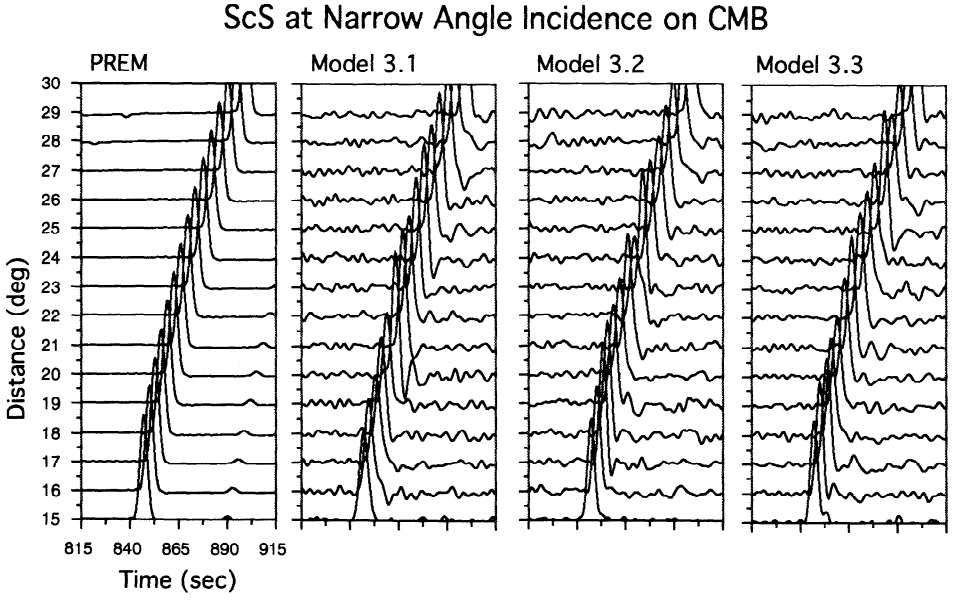

Figure 9. *SH* displacement synthetic seismograms for three realizations of model 3 for the *ScS* waveform in the distance range 15° to 30°.

tives must operate over a period of time sufficient to provide a mechanism of recharge for a D" discontinuity.

4.2. Implications for Seismic Attenuation in D"

Synthetic seismograms for heterogeneous models of the lower mantle have shown that *ScS* and *PcP* waveforms can be considerably broadened by scattering in D". The pulse broadening of *PcP* and *ScS* caused by D" heterogeneity suggests that care must be taken in interpreting *PcP* and *ScS* pulse broadening as the result of intrinsic anelasticity. Reasonable levels of D" heterogeneity, entirely consistent with the power of scattered *PKIKP* precursors, predict enough broadening of *PcP* and *ScS* waveforms that any additional contribution to pulse broadening by a high intrinsic attenuation (low Q) zone in D" would to be inconsistent with observed waveforms. Unless partial melt occurs in D", the high lithostatic pressure near the core-mantle boundary may be sufficient to dominate the effect of increased temperature in a thermal boundary layer. These conditions may prevent the movement of the relaxation spectrum of anelasticity into the high-frequency body wave band [*Lundquist and Cormier,* 1980; *Anderson and Given,* 1982].

4.3. Evidence for Entrainment of Small-Scale Heterogeneity

The magnitude of small-scale heterogeneity of D" evident from the waveforms of both long-period and short-period data is too large to be consistent with a thermal origin. In the wavenumber band 0.0001 to 0.002 km^{-1} the heterogeneity statistics of both regional and global tomographic studies agree with a power law decay in wavenumber of velocity heterogeneity on the order of -2 to -3 [*Chevrot et al.*, 1998]. Powers of -2 to -3 are consistent with the predictions for the shape of the heterogeneity spectrum caused by temperature variations in the viscous-convective regime of a convecting fluid. A k^{-2} behavior of the heterogeneity spectrum is sometimes termed Batchelor or Kolmolgorov scaling in theories of the heterogeneous structure of convecting atmospheres or oceans [*Hill,* 1978]. At a sufficiently high wavenumber, corresponding to the spatial scale at which the timescale of heat transport by diffusion overtakes the timescale of heat transport by convection, the shape of the heterospectrum changes. In the vicinity of this critical wavenumber the k^{-2} domain transforms to a domain of much stronger exponential decay with k. This transformation may possibly explain the reddening of the heterospectrum of D" observed in tomographic studies in the wavenumber band up to 0.002 km^{-1}. The power of D" heterogeneity observed with short-period body waves, however, is far too high to be consistent with a continuation of reddening between the 0.002 and 1 km^{-1} wavenumber band. Thus, if a thermal origin of heterogeneity were assumed for scale lengths as small as 10 km, the heterogeneity power would be too small to account for the coda power between *S* and *ScS* as well as the power of *PKIKP* precursors. An assumption of exponential scaling in this low wavenumber band gives even a worse fit to observations.

It is more likely that the small-scale (100 km and smaller) heterogeneities of the lower mantle are chemical rather than thermal in origin. The shape of the late coda of scattered precursors to*PKIKP* suggests that at least the lower 1000 km of the mantle is characterized by a pervasive entrainment of small-scale chemical heterogeneities in larger-scale convective motions [*Hedlin et al.,* 1997]. Assuming a mantle viscosity of 10^{21} Pa s, a density contrast of 1 g/cm, and convective velocity of 1 cm/yr, *Turcotte and Schubert* [1982] show that spherical heterogeneities having a radius of 38 km or smaller can be entrained in mantle flow. Similar sized heterogeneities having smaller density contrasts, consistent with the neglect of density perturbations in the modeling of this paper, should be even more easily entrained.

The hypothesis that the D" discontinuity may result from a change in the statistics of small-scale heterogeneity has important consequences for our understanding of mantle dynamics, not necessarily requiring the existence of a thick, relatively homogeneous, chemically distinct or solid phase changed layer at the lower mantle. Small-scale, entrained, chemical heterogeneity may be due to the presence of horizontally elongated lenses of partial melt, horizontally oriented remnant slab fragments, or thin lenses of core-mantle reaction products. Another possibility is that the change in the heterogeneity spectrum may be simply caused by a gradual transition in homologous temperature (T/T_m, where T_m is melting temperature). The higher homologous temperature would decrease viscosity and reset the amplitude of a heterospectrum whose shape with wavenumber would not change much compared to that of the overlying mantle. Such a viscosity change could also affect the heterogeneity spectrum by resetting the entrainment constraints on small-scale heterogeneity.

Continued numerical modeling of seismic body waves, including *P* and *SV* waves at varying ranges, interacting with a variety of statistically described heterogeneity in the lower mantle will help narrow these possibilities, together with the imaging techniques of exploration seismology made possible by dense 2- and 3-D arrays.

5. Conclusions

5.1. *SdS* and *PdP*

Results of numerical modeling show that the observations of the D" discontinuity can agree with the effects of a diffuse transition in heterogeneity statistics. Of the three types of changes in the heterogeneity statistics of the lowermost mantle investigated, a simple extrapolation of tomographically resolved heterogeneity to short wavelengths works best in predicting *SdS* arrivals. Not all realizations of this statistical model, however, pro-

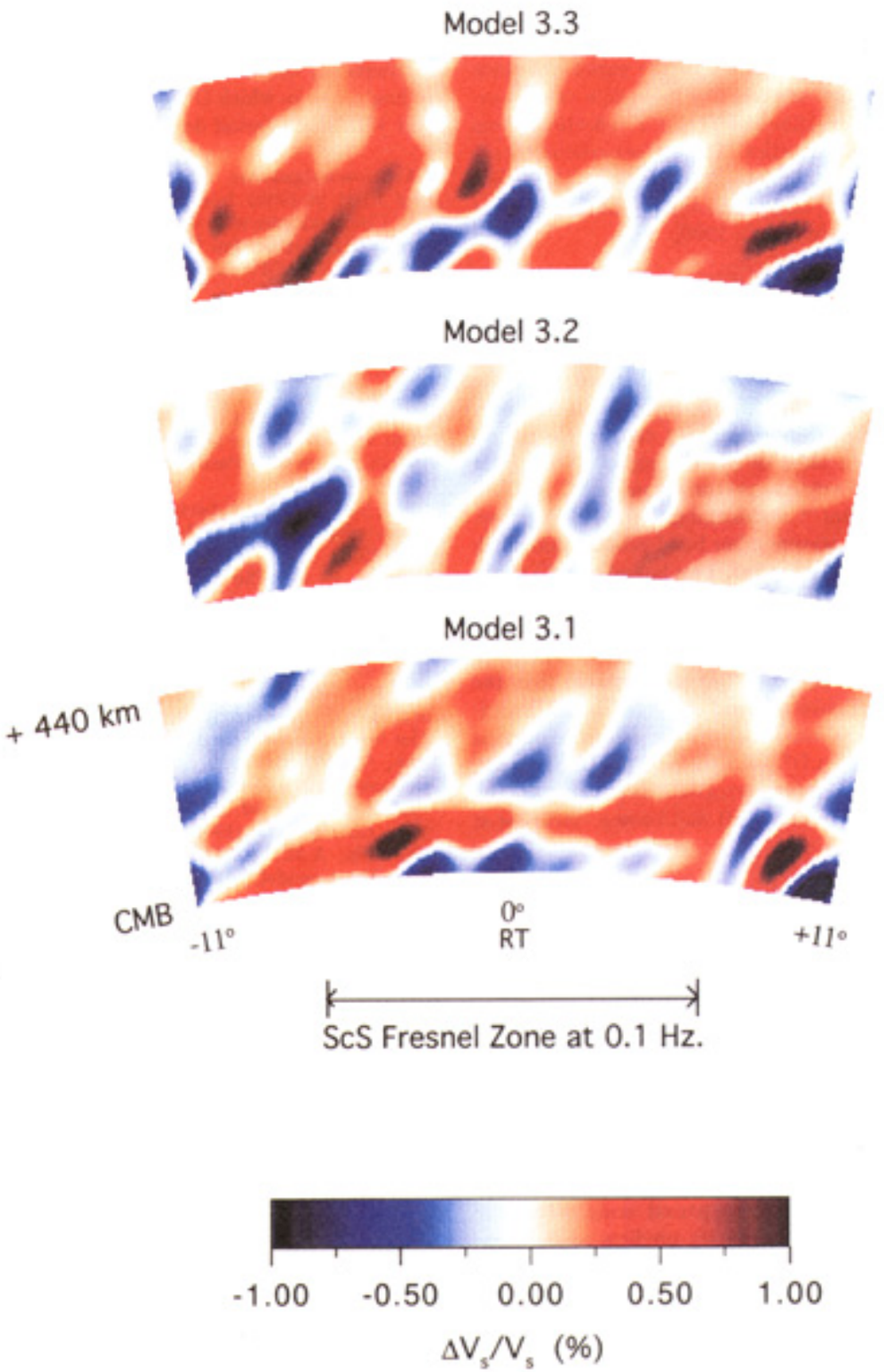

Plate 2. Low-pass-filtered images of three different realizations of the model 3 heterogeneity spectrum. The approximate width of the Fresnel zone for a 0.1 Hz *ScS* wave is shown.

duce *SdS* arrivals. A minimum requirement for *SdS* excitation seems to be the existence of elongated high-velocity anomalies, embedded in a low-velocity region, roughly parallel to the core-mantle boundary. Strong, three-dimensional, topography of the surface of these elongated anomalies is necessary to explain the behavior of global observations of P and S reflections from apparent D" discontinuities. These observations are occasionally strong at high angles of incidence [*Schimmel and Paulssen,* 1996] and arrive significantly off a great circle azimuth [*Weber et al.,* 1996].

5.2. Anisotropy and Heterogeneity Bounds

An onset of anisotropy of scale lengths of heterogeneity in D" is permitted but not required by data consisting of *PKIKP* precursors and broadband *SH* waves grazing the CMB. Some firm bounds on the intensity of P and S velocity heterogeneity can be clearly established through most of the D" region. The upper bound to RMS S velocity perturbations in D" is 3% in the 0.0001 to 1 km^{-1} wavenumber band. Higher perturbations in this wavenumber band produce too much scattering attenuation in *ScS*. This bound in $\Delta V_S/V_S$ is too low to account for observed shear wave anisotropy in core grazing S waves by a mechanism of shape preferred anisotropy [*Kendall and Silver,* 1998]. The RMS variation can be a factor of 2 or more smaller than the peak variation. Hence a bound of 3% on the RMS variation can still be consistent with the existence of ultra low-velocity zones in D" [e.g., *Garnero and Helmberger,* 1995] having much larger perturbations as along as they are located right at the CMB and have a thickness < 50 km.

5.3. D" Heterogeneity Spectrum

Some reddening in the D" spectrum occurs in the low (0.0001 to 0.002) wavenumber band of tomographic images and agrees with the expectations for a convecting homogeneous mantle. A mechanism must exist, however, to reduce or cancel the decay of the power of heterogeneity in the 0.002 to 1 km^{-1} wavenumber band with increasing wavenumber predicted from thermal variations in a convecting mantle. A likely mechanism is entrainment of small-scale (10-100 km sized) chemical heterogeneities in mantle flow.

From the modeling of long-period body waves the preferred model of heterogeneity predicts a slight enrichment of small scale lengths in D". This seems to be in conflict with a result of *Hedlin et al.* [1997], who prefer a more uniform distribution of heterogeneity in the lower 1000 km of the mantle to agree with the shape of the coda of *PKIKP* precursors. The enrichment of small scale heterogeneity in D", however, is sufficiently small that it would be barely discernable in stacked bins of *PKIKP* precursors. An enrichment of small scale heterogeneity in D" may account for the slight discrepancy described by *Shearer et al.* [1998] between the observed amplitude of *PKIKP* precursor coda amplitude at short range (130°) and that predicted by uniform models of heterogeneity. Nonetheless, the experiments in this paper show that is not difficult to construct a D" model having an apparent thickness that differs depending on the frequency content of the wave field sampling it, including a case in which D" is not even visible as distinct layer with short-period data.

Acknowledgments. This research was supported by grant EAR 96-14525 from the National Science Foundation. Computations were supported by an allocation from the National Partnership for Computational Infrastructure (NPACI) at NPACI's site at UCSD.

References

Anderson, D.L., and J.W. Given, Absorption band Q model for the Earth, *J. Geophys. Res., 87*, 3893-3904, 1982.

Bataille, K., R.S. Wu, and S.M. Flatte, Inhomogeneities near the core-mantle boundary evidenced from scattered waves: A review, *Pure Appl. Geophys., 132*, 151-173, 1990.

Blanch, J.O., J.O.A, Robertsson, and W.W. Symes, Optimally efficient constant-Q modeling, *Geophysics, 60*, 176-184, 1995.

Chapman, C. H., The Earth flattening transformation in body wave theory, *Geophys. J. R. Astron. Soc., 35*, 55-80, 1973.

Chevrot, S., J.-P. Montagner, and R. K. Snieder, The spectrum of tomographic Earth models, *Geophys. J. Int., 133*, 783-788, 1998.

Cormier, V.F., Anisotropy of heterogeneity scale lengths in the lower mantle from PKIKP precursors, *Geophys. J. Int., 136*, 373-384, 1999.

Dziewonski, A.M., Global seismic tomography of the mantle, *U.S. Nat. Rep. Int. Union Geod. Geophys. 1991-1994, Rev. Geophys., 33*, 419-433, 1995.

Dziewonski, A.M., and D.L. Anderson, Preliminary reference Earth model, *Phys. Earth Planet. Inter., 25*, 3295-3314, 1981.

Fornberg, B.,*A Practical Guide to Pseudospectral Methods*, Cambridge Univ. Press, New York, 1996.

Furumura, T., and H. Takenaka, A wraparound elimination technique for the pseudospectral wave synthesis using an antiperiodic extension of the wavefield, *Geophysics, 60*, 302-307, 1995.

Furumura, T., B.L.N. Kennett, and M. Furumura, Seismic wavefield calculation for laterally heterogeneous whole Earth models using the pseudospectral method, *Geophys. J. Int., 135*, 845-860, 1998.

Frankel, A., and R.W. Clayton, Finite difference simulations of seismic scattering: Implications for the propagation of short-period seismic waves in the crust and models of crustal heterogeneity, *J. Geophys. Res., 91*, 6465-6489, 1986.

Garnero, E.J., and D.V. Helmberger, A very slow basal layer underlying large scale low-velocity anomalies in the lower mantle beneath the Pacific: Evidence from core-phases, *Phys. Earth. Planet. Inter., 91*, 161-176, 1995.

Haddon, R.A.W., and G.G.R. Buchbinder, S-wave scattering by 3-D heterogeneities at the base of the mantle, *Geophys. Res. Lett., 14*, 891-894, 1987.

Hedlin, M.A.H., P.M. Shearer, and P.S. Earle, Waveform stacks of *PKP* precursors: Evidience of small-scale heterogeneity throughout the mantle, *Nature, 387*, 145-150, 1997.

Hill, R.J., Models of the scalar spectrum for turbulent advection, *J. Fluid Mech., 88*, 541-562, 1978.

Igel, H., and M. Weber, *P-SV* wave propagation in the Earth's mantle using finite differences: Application to heterogeneous lowermost mantle structure, *Geophys. Res. Lett.*, *23*, 415-418, 1996.

Kellogg, L.H., Growing the Earth's D" layer: Effect of density variations at the core-mantle boundary, *Geophys. Res. Lett.*, *24*, 2749-2752, 1997.

Kendall, J.M., and P.G. Silver, Investigating causes of D" anisotropy, *The Core-Mantle Boundary Region, Geodyn. Ser.*, vol. 28, editied by M. Gurnis et al., pp. 97-118, AGU, Washington, D.C., 1998.

Kosloff, D., and D. Kessler, Seismic numerical modeling, *Oceanographic and Geophysical Tomography*, edited by Y. Desaubies, A. Tarantola, and J. Zinn- Justin, pp. 249-312, North-Holland, New York, 1990.

Lay, T., and D.V. Helmberger, A lower mantle *S*-wave triplication and the shear velocity structure of D", *Geophys. J. R. Astron. Soc.*, *75*, 799-837, 1983.

Li, X-D., and B. Romanowicz, Global shear velocity model developed using nonlinear asymptotic coupling theory, *J. Geophys. Res.*, *101*, 22,245-22,273, 1996.

Lundquist, G.M., and V.F. Cormier, Constraints on the absorption band model of *Q*, *J. Geophys. Res.*, *85*, 5244-5256, 1980.

Richards, P.G., and W. Menke, The apparent attenuation of a scattering medium, *Bull. Seismol. Soc. Am.*, *73*, 1005-1021, 1983.

Robertsson, J.O.A., J.O. Blanch, and W.W. Symes, Viscoelastic finite-difference modeling, *Geophysics*, *59*, 1444-1456, 1994.

Schimmel, M., and H. Paulssen, Steeply reflected *ScSH* precursors from the D" region, *J. Geophys. Res.*, *101*, 16,077-16,087, 1996.

Shearer, P.M., M.A.H. Hedlin, and P.S. Earle, *PKP* and *PKKP* precursor observations: Implications for the small-scale structure of the deep mantle and core, *The Core-Mantle Boundary Region, Geodyn. Ser.*, vol. 28, editied by M. Gurnis et al., pp. 37-55, AGU, Washington, D.C., 1998.

Sidorin I, M. Gurnis, V. Helmberger, Evidence for a ubiquitous seismic discontinuity at the base of the mantle, *Science*, *286*, 1326-1331, 1999.

Snir, M., S. Otto, S. Huss-Lederman, D. Walker, and J. Dongarra, *MPI: The Complete Reference*, vol. 1, 2nd ed., MIT Press, Cambridge, Mass., 1998.

Su, W., R. L. Woodward, A.M. Dziewonski, Degree 12 model of shear velocity heterogeneity in the mantle, *J. Geophys. Res.*, *99*, 6945-6980, 1994.

Tackley, P.J., Three-dimensional simulations of mantle convection with a thermo-chemical basal boundary layer: D"? *The Core-Mantle Boundary Region, Geodyn. Ser.*, vol. 28, editied by M. Gurnis et al., pp. 231-253, AGU, Washington, D.C., 1998.

Turcotte, D.L., and G. Schubert, Heat Transfer, in *Geodynamics*, p. 267, John Wiley, New York, 1982.

Virieux, J., *P-SV* wave propagation in heterogeneous media: Velocity stress finite-difference method, *Geophysics*, *51*, 889-901, 1986.

Weber, J., J.P. Davis, C. Thomas, F. Kruger, F. Scherbaum, J. Schlittenhardt, and M. Kornig, The structure of the lowermost mantle as determined from seismic arrays, in *Seismic Modelling of the Earths Structure*, edited by E. Boschi, G. Ekstrom, and A. Morelli, pp. 399-342, Ist. Naz. di Geophys., Rome, 1996.

Witte, D., The pseudospectral method for simulating wave propagation, Ph.D. thesis, Columbia Univ., New York, 1985.

Wysession, M.E., T. Lay, J. Revenaugh, Q. Williams, E.J. Garnero, R. Jeanloz, and L. H. Kellogg, The D" discontinuity and its implications, *The Core-Mantle Boundary Region, Geodyn. Ser.*,vol. 28, editied by M. Gurnis et al., pp. 273-297, AGU, Washington, D.C., 1998.

V.F. Cormier, University of Connecticut, Department of Geology and Geophysics, 354 Mansfield Road, Room 207, U-45, Storrs, CT 06269-2045. (e-mail: cormier@geol.uconn.edu)

(Received September 3, 1999; revised February 18, 2000; accepted April 13, 2000.)